Temperature Calibration of Elevated Mg/Ca in Planktic Foraminifera Shells From the Hypersaline Gulf of Aqaba

N. Levy[1,2] ⬤, A. Torfstein[2,3] ⬤, R. Schiebel[1] ⬤, N. Chernihovsky[2,3], K. P. Jochum[1], U. Weis[1] ⬤, B. Stoll[1], and G. H. Haug[1,4]

[1]Max Planck Institute for Chemistry, Mainz, Germany, [2]The Fredy & Nadine Herrmann Institute of Earth Sciences, Hebrew University of Jerusalem, Jerusalem, Israel, [3]Interuniversity Institute for Marine Sciences, Eilat, Israel, [4]Department of Earth Sciences, ETH Zurich, Zurich, Switzerland

Abstract The Mg/Ca of marine calcareous Planktic Foraminifera (PF) shells is commonly used for sea surface temperature reconstructions. However, compared to open marine environments, hypersaline (>40) oligotrophic seas have been shown to accommodate PF with higher Mg/Ca and divergent temperature to Mg/Ca relationships. To investigate influencing factors of PF Mg uptake in hypersaline regions, we measured the Mg/Ca of two flux-dominating PF species, *Globigerinoides ruber albus* and *Turborotalita clarkei*, derived from a monthly resolved time series of sediment traps in the Gulf of Aqaba, northern Red Sea as well as the corresponding temperature, salinity, and *p*H values. The PF exhibit elevated Mg/Ca which cannot be explained by post-deposition or interstitial sediment diagenetic processes. *G. ruber albus* displays Mg/Ca trends that strongly follow seasonal mixed layer temperature changes. Conversely, *T. clarkei* Mg/Ca trends do not follow temperature but rather show significant Mg/Ca enrichment following mixing of the surface water column. We present a framework for incorporating elevated Mg/Ca into global Mg/Ca-T calibrations for *G. ruber albus* and present a new Mg/Ca-T calibration suitable for hypersaline marine environments.

Plain Language Summary Past seawater temperature is reconstructed from the magnesium-to-calcium ratio (Mg/Ca) in the calcareous shells of a group of marine microplankton called foraminifera. Two foraminifer species, *Globigerinoides ruber albus* and *Turborotalita clarkei*, are abundant in the Gulf of Aqaba, northern Red Sea, at year-round high temperatures and salinities. The shells of these foraminifera have elevated Mg/Ca relative to other marine regions, and here, we explore the factors causing this. The Mg/Ca values of both *G. ruber albus* and *T. clarkei* reflect the environmental conditions of the water column. For *G. ruber albus*, temperature and salinity appear to be factors responsible for the Mg/Ca trends and elevated values. We incorporate the new Mg/Ca data for *G. ruber albus* to calibrate elevated Mg/Ca with temperature for high-salinity (>40) marine environments. The Mg/Ca of the deeper dwelling *T. clarkei* show higher ratios following deep mixing of the surface water column and may indicate annually recurring phytoplankton blooms caused by nutrient input into the sunlit ocean surface.

1. Introduction

1.1. Trace Element Chemistry of Planktic Foraminifera (PF) Shells

Planktic Foraminifera (PF) shells are instrumental in the study of the history of Earth's climate and oceans (e.g., Berggren et al., 1995; Gupta, 1999; Kucera, 2007; Rosenthal, 2007; Schiebel, 2002; Schiebel & Hemleben, 2017). The PF shells capture water column conditions during calcification as shown by the trace element ratios in the calcium carbonate (Katz et al., 2010; Lea, 1999; Mortyn & Martínez-Botí, 2007). Of these, the Mg/Ca of PF shells is a widely applied tracer of past surface seawater temperatures (e.g., Allen et al., 2016; Elderfield & Ganssen, 2000; Elderfield et al., 2002; Evans et al., 2018; Friedrich et al., 2012; Hastings et al., 1998; Lea et al., 1999; Nürnberg et al., 1996; Rosenthal et al., 1997; Wefer et al., 1999). Paleo-temperature reconstructions apply Mg/Ca-T calibrations derived empirically from modern PF shells, which commonly display a positive relationship, that is, increasing Mg/Ca with increasing water temperature (e.g., Anand et al., 2003; Cléroux et al., 2008; Elderfield & Ganssen, 2000).

The trace element composition of PF can be misinterpreted when ecological requirements at the species level and specific regional characteristics are not considered. Assuming a positive Mg/Ca-T relationship, deeper dwelling PF will incorporate less Mg into their shell relative to shallow dwelling species due to temperature differences.
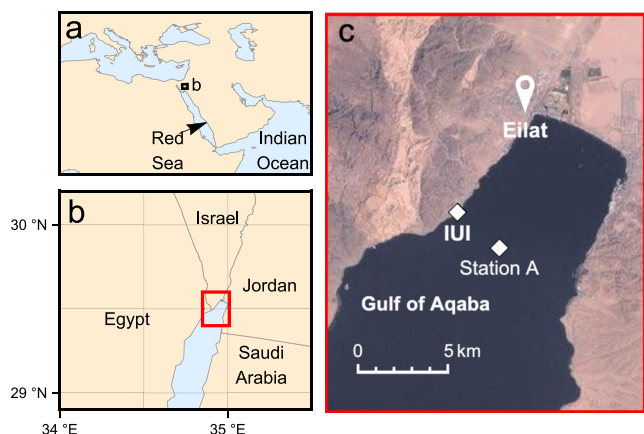
Figure 1. Location maps. (a) Red Sea, (b) northern Gulf of Aqaba (GOA), and (c) satellite image of the northern tip of the GOA, displaying the location of the Interuniversity Institute (IUI) for Marine Sciences. *Station A* is a long-term monitoring site located around 4 km off shore where water depths reach ~700 m (Meeder et al., 2012). A permanent bottom-tethered mooring mounted with vertically stacked sediment traps is deployed proximal to *Station A* at 610 m (Torfstein et al., 2020).

Although temperature is assumed the predominant control on the Mg content of PF shells, other oceanographic parameters such as salinity and *p*H can control Mg/Ca (Arbuszewski et al., 2010; Broecker & Clark., 1999; Dissard et al., 2010; Dueñas-Bohórquez et al., 2009; Evans, Brierley, et al., 2016; Evans, Wade, et al., 2016; Ferguson et al., 2008; Gray & Evans, 2019; Gray et al., 2018; Hönisch et al., 2013; Hoogakker et al., 2009; Kisakürek et al., 2008; Lea et al., 1999; Le Houedec et al., 2021; Mathien-Blard & Bassinot, 2009; Sadekov et al., 2009; Saenger & Evans, 2019). Additionally, biological effects and processes of remineralization and dissolution during sedimentation add complexity to the understanding of the behavior of proxies in different species (Bijma et al., 2002; Eggins et al., 2003; Johnstone et al., 2011; Lea et al., 1999; Nürnberg et al., 1996; Regenberg et al., 2006, 2014).

In most marine environments, the Mg/Ca in PF varies between ~0.5 and 5 mmol/mol (Gupta, 1999; Schiebel & Hemleben, 2017). Higher Mg/Ca values have been measured in PF shells from higher salinity (>36.8) oligotrophic basins such as the Red Sea (Hoogakker et al., 2009; Mezger et al., 2018) and the Mediterranean Sea (Boussetta et al., 2011; Ferguson et al., 2008; Sabbatini et al., 2011). Mg/Ca from core tops in the Mediterranean Sea was reported in the range of 2.6–10.3 mmol/mol, with some measurements reaching up to 35.5 mmol/mol (Boussetta et al., 2011; Ferguson et al., 2008; Sabbatini et al., 2011). In the more saline Eastern Mediterranean, Mg/Ca in core tops are generally higher than 10 mmol/mol. It has been suggested that the elevated Mg/Ca values in these high salinity regions may result from recrystallization on the PF shells occurring at the sediment water interface (Hoogakker et al., 2009), a process which raises the question whether Mg/Ca can be used as a proxy for sea surface temperature reconstruction in hypersaline environments. In global calibration models, elevated Mg/Ca PF data from hypersaline environments are commonly excluded (e.g., Anand et al., 2003; Gray et al., 2018; Tierney et al., 2019). However, the exclusion of Mg/Ca PF from hypersaline environments from global calibrations cannot be justified when considering the large global ocean salinity changes which occurred in the geological past. It is thus critical that the dynamics of Mg incorporation into PF shells in hypersaline environment is thoroughly assessed. Specifically, it is still not clear whether elevated Mg/Ca values in PF reflect Mg incorporation in situ in the hypersaline water column or in the water-sediment interface. In turn, this hampers the application of Mg/Ca as a proxy for temperature in hypersaline environments and its implementation into global temperature calibrations.

1.2. Study Area and Site Background

The Gulf of Aqaba (GOA), northern Red Sea, is considered to be a "natural marine laboratory" and an accessible open ocean proxy environment (Benaltabet et al., 2020; Biton & Gildor, 2011; Chase et al., 2011; Lazar et al., 2008; Meeder et al., 2012; Paytan et al., 2009; Reiss & Hottinger, 1984; Torfstein & Kienast, 2018). It is approximately 180 km long, 10–25 km wide, with very steep margins, an average depth of 800 m at its northern end, and a maximum depth of 1,830 m (Figure 1). The regional climate is hyper-arid (mean annual rainfall <30 mm), resulting in limited direct input of terrigenous material into the GOA from surface runoff waters (Chase et al., 2011; Ganor & Foner, 2001; Katz et al., 2015; Reiss & Hottinger, 1984; Torfstein et al., 2017). The main source of trace metals to the surface waters is from settling atmospheric dust (Chen et al., 2008).

The GOA is characterized by very high evaporation-driven salinity (~40.5) as well as large seasonal sea surface temperature variations (Biton & Gildor, 2011). These conditions result in seasonal summer stratification and winter mixing (Meeder et al., 2012). Bottom waters display a constant temperature of ca. 20°C. During summer, surface waters can reach >29°C (Figure 2). Throughout autumn and winter, the surface water cools and becomes denser, resulting in deepening of the mixed layer until a maximum depth is reached in later winter and spring. Typically, the maximum mixing depth is ~300–400 m, but every several year the mixing depth can reach 700 m or more.

1.3. Ecology of Planktic Foraminifera in the GOA

The high salinity together with the large surface water temperature variations make the PF ecology in the GOA sensitive to seasonal temperature changes and a suitable study site to investigate the incorporation of Mg/Ca in
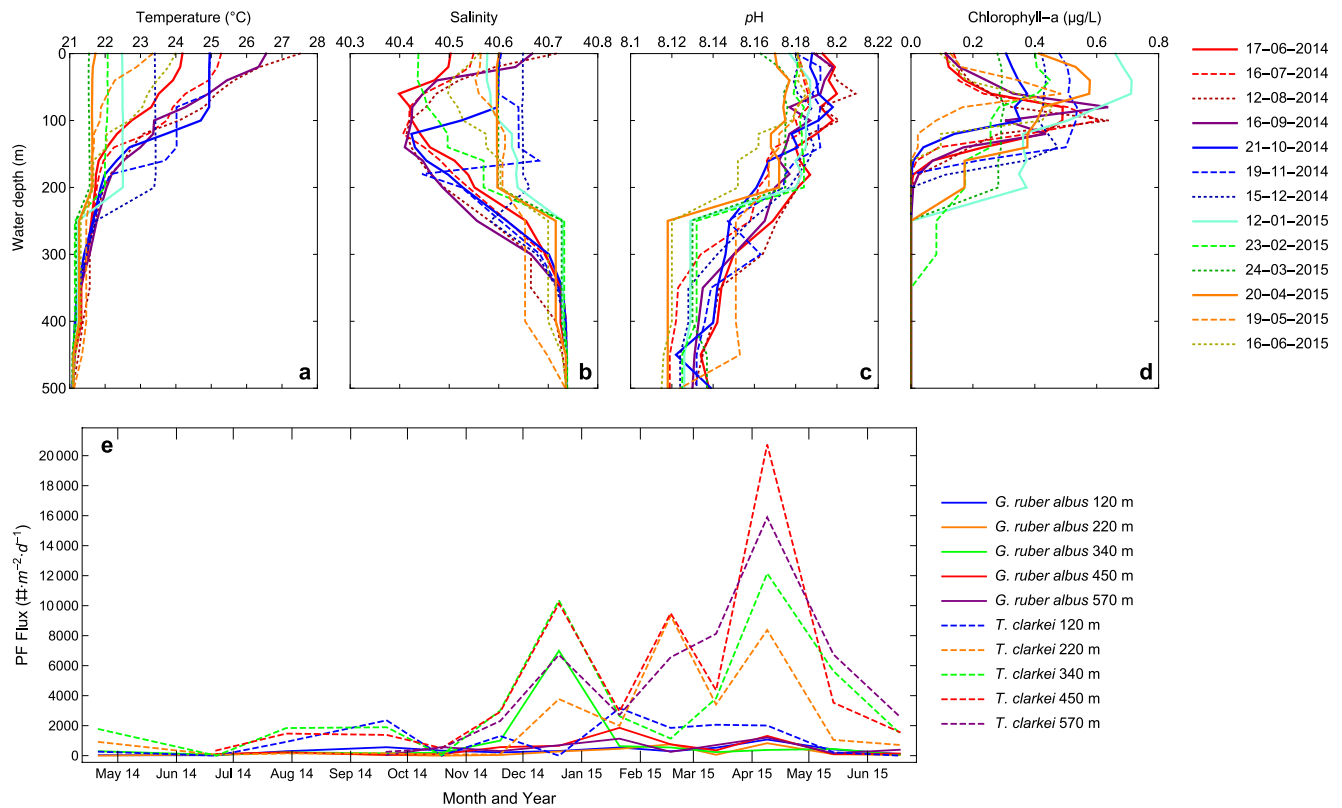
Figure 2. *Station A* depth profiles of monthly measured (a) temperature, (b) salinity, (c) *p*H, and (d) chlorophyll-*α* concentrations (data from the Israel National Monitoring Program; Shaked & Genin, 2016) as well as (e) PF flux time-series during 2014–2015 from five vertically stacked sediment traps deployed proximal to *Station A* (data from Chernihovsky et al. (2018)).

PF shells in hypersaline environments. Total PF fluxes demonstrate strong seasonality, with low values observed during summer months and gradually increasing during the autumn-winter (Chernihovsky et al., 2018, Figure 2e). This increase is coeval with decreasing sea-surface temperatures and deepening of the mixed layer depth (MLD) that drives the admixture of nutrient-replete subsurface waters into the mixed layer. Spinose species constitute the majority of the PF assemblage in the GOA. The dominant shell size-fraction is between 63 and 125 μm (~86% of the total flux), which has generally been overlooked in previous studies, resulting in a significant knowledge gap related to the early ontogenetic stages of large-sized species and the small-sized PF species (Brummer et al., 1986; Chernihovsky et al., 2018). The 63–125 μm shell size-fraction is dominated by the small species *T. clarkei*, and the >125 μm size-fraction is dominated by the species *G. ruber albus* (Chernihovsky et al., 2018; Morard et al., 2019). *Globigerinoides ruber albus* bears dinoflagellate symbionts, dwells in the surface sunlit ocean, and prospers in a wide range of temperatures (14–31°C) and salinities of 22–49 (Bijma et al., 1990). It is abundant in oceanic tropical and sub-tropical gyres and is commonly applied as a paleo-thermometer in downcore studies (e.g., Gray & Evans, 2019; O'Brien et al., 2014; Schiebel et al., 2004). *Turborotalita clarkei* is a symbiont-barren species that occupies tropical to temperate waters, but has been fairly overlooked in many studies, and some aspects of its ecological requirements are still unknown (Boltovskoy, 1991; Chernihovsky et al., 2018).

In this study, we investigate the Mg/Ca dynamics in the calcareous shells of the flux dominating PF in the GOA, picked from sediment traps and determine the dominant factors for Mg/Ca incorporation in PF. We explore the spatial and temporal Mg/Ca changes in two species (*G. ruber albus* and *T. clarkei*) and corresponding oceanographic parameter trends (temperature, salinity, *p*H) over different water column depths at monthly resolutions during 2014–2015 (Table 1). We further assess whether Mg/Ca in these species can be used as a water column temperature proxy in hypersaline seas and incorporated into local and global Mg/Ca-T calibrations.

Table 1
Monthly Mixed Layer Depth (MLD), and Mean Temperatures, Salinities, and pH in the Surface Mixed Layer

	MLD (m)	T (°C)	S	pH
Date				
13 May 2014	40	23.5 ± 0.1	40.40 ± 0.01	8.18 ± 0.00
17 June 2014	60	24.1 ± 0.1	40.49 ± 0.02	8.20 ± 0.00
16 July 2014	60	25.1 ± 0.2	40.53 ± 0.03	8.18 ± 0.00
12 August 2014	20	27.5 ± 0.0	40.72 ± 0.00	8.19 ± 0.00
16 September 2014	40	26.4 ± 0.2	40.65 ± 0.02	8.19 ± 0.01
21 October 2014	120	24.9 ± 0.1	40.59 ± 0.03	8.19 ± 0.00
19 November 2014	80	25.0 ± 0.0	40.60 ± 0.00	8.19 ± 0.01
15 December 2014	250	23.4 ± 0.0	40.65 ± 0.00	8.18 ± 0.00
12 January 2015	250	22.5 ± 0.0	40.61 ± 0.03	8.18 ± 0.00
23 February 2015	160	22.1 ± 0.0	40.46 ± 0.03	8.18 ± 0.00
24 March 2015	250	21.5 ± 0.0	40.60 ± 0.00	8.17 ± 0.00
20 April 2015	250	21.6 ± 0.0	40.60 ± 0.00	8.17 ± 0.00
19 May 2015	20	23.3 ± 0.0	40.56 ± 0.00	8.18 ± 0.00
16 June 2015	60	23.7 ± 0.3	40.53 ± 0.03	8.18 ± 0.00
14 July 2015	40	25.7 ± 0.2	40.70 ± 0.01	8.18 ± 0.00
18 August 2015	40	26.8 ± 0.4	40.70 ± 0.06	8.19 ± 0.00

Note. Measuring dates and mean values of temperatures (T), salinities (S), and pH at *Station A* (Shaked & Genin, 2016). MLD gives mixed layer depth in meters. Italic numbers are standard deviation.

2. Materials and Methods

2.1. Sampling and Oceanographic Data

A bottom-tethered mooring has been deployed continuously since January 2014 near *Station A* in the northern part of the GOA, 29° 28′95′N, 34° 56′22′E, ~610 m water depth (Figure 1). The mooring consists of KC Denmark cylinder traps vertically stacked at five different depths, 120, 220, 340, 450, and 570 m, that were collected at an approximate monthly resolution (Table 2). A detailed description of the mooring, sampling, sample processing, and trapping efficiencies can be found in Chernihovsky et al. (2018) and Torfstein et al. (2020). The PF shells were picked from the monthly bulk samples collected between June 2014 and July 2015 (Chernihovsky et al., 2018).

A core top sample (0–1 cm) was collected from the GOA seafloor at *Station A*, using a MC-400 four-barrel multi-corer (Ocean Instruments, San Diego, CA). The sample was wet-sieved at 63 μm, oven-dried at 40°C and dry-sieved with various mesh-size sieves (100 and 250 μm) at the Max Planck Institute for Chemistry.

Hydrologic data is obtained routinely at *Station A* by the Israel National Monitoring Program (NMP, Shaked & Genin, 2016), including sea surface and water column temperature (°C), salinity, oxygen concentrations (μmol/l), alkalinity (meq/kg), pH, and chlorophyll-α concentrations (μg/l). The potential density anomaly was calculated based on temperature, salinity, and pressure at the surface ($\sigma 0_{(surface)}$) and all respective water column depths (in 20 m interval resolution). The MLD has been defined as the water depth where the density anomaly ($\sigma 0$) is equal to, or above, the water density of the surface water column plus the density threshold of 0.125 kg/m³ (Sprintall & Tomczak, 1992). Mean values of temperature, salinity, and pH were calculated for all measured depths above the MLD (Table 1).

2.2. Species Classification and Preparation for LA-ICP-MS

Identification of the PF taxa followed Schiebel and Hemleben (2017) and Morard et al. (2019). For each month between June 2014 and June 2015, three clean, translucent individuals without dried cytoplasm or sediment residues were picked from the five sediment traps between 120 and 570 m water depths. Preliminary preparation and cleaning steps, such as rinsing with ultrapure water to remove salts, are described by Chernihovsky et al. (2018). A single chamber, individual foraminifer analysis was conducted using Laser Ablation Inductively Coupled Plasma Mass Spectrometry (LA-ICP-MS; see Section 2.3) on 156 specimens of the two morphotypes of *T. clarkei* "big" and "encrusted," and *G. ruber albus* (i.e., *G. ruber* sensu stricto (s.s.), white) to account for population variability (Fehrenbacher et al., 2020) and inter chamber variability. The *G. ruber albus* tests are generally larger than the *T. clarkei* tests. From the two *T. clarkei* phenotypes that were picked, one is larger (labeled "big") and all chambers are fully recognizable. The other *T. clarkei* was overall smaller and "encrusted" with an egg-shaped test. The chambers of *T. clarkei* "encrusted" are harder to distinguish compared to *T. clarkei* "big." Samples were mounted on a glass slide with a methyl-hydroxy-propyl-cellulose (MHPC 1:100) glue. Reductive and oxidative cleaning were not applied on any sample to preserve the original signals related to different stages in the PF life cycle and encrustation process, and any outer layers of the shell that are added during ontogeny (Jochum et al., 2019; Schiebel & Hemleben, 2017). This is important for *T. clarkei*, as reductive and oxidative cleaning may result in the loss of a significant part of shell material of its 1.9–3.6 μm thin shells (measured from Scanning Electron Microscopy (SEM) images including Figure 3).

2.3. LA-ICP-MS and Data Processing

Analyses of the calcium-normalized magnesium (Mg/Ca) and strontium (Sr/Ca) abundances were conducted using a 200 nm wavelength NWR femtosecond (fs) LASER system from ESI, combined with a sector-field

Table 2
Monthly Mean Mg/Ca for G. ruber albus, T. clarkei "Big" and T. clarkei "Encrusted"

Month	Year	Start	End	Mg/Ca G. ruber albus	n	Mg/Ca T. clarkei "big"	n	Mg/Ca T. clarkei "encrusted"	n
June	2014	02-06-2014	13-07-2014	8.48 ± *1.81*	4	8.37 ± *1.09*	*1	24.93 ± *22.72*	*1
July	2014	13-07-2014	14-08-2014	12.17 ± *2.83*	4	7.40 ± *2.07*	3	7.56 ± *0.26*	3
September	2014	09-09-2014	02-10-2014	10.15 ± *3.32*	4	7.31 ± *0.87*	4	13.41 ± *10.64*	3
October	2014	02-10-2014	06-11-2014	7.98 ± *0.97*	3	10.01 ± *5.07*	4	9.12 ± *2.28*	2
November	2014	06-11-2014	03-12-2014	6.25 ± *1.86*	4	9.29 ± *3.51*	3	7.21 ± *0.86*	3
December	2014	03-12-2014	06-01-2015	7.20 ± *0.48*	4	6.47 ± *1.35*	3	10.04 ± *1.98*	4
January	2015	08-01-2015	03-02-2015	7.00 ± *2.11*	4	8.89 ± *3.64*	4	9.31 ± *1.75*	4
February	2015	03-02-2015	03-03-2015	5.20 ± *0.93*	4	8.45 ± *2.41*	4	8.25 ± *2.03*	4
March	2015	03-03-2015	23-03-2015	5.47 ± *0.69*	4	21.28 ± *14.35*	4	16.87 ± *11.23*	4
April	2015	23-03-2015	26-04-2015	8.38 ± *1.54*	3	26.59 ± *10.83*	4	16.49 ± *7.33*	3
May	2015	26-04-2015	02-06-2015	6.61 ± *2.90*	4	15.63 ± *8.07*	4	10.78 ± *1.88*	3
June	2015	02-06-2015	05-07-2015	6.39 ± *1.74*	4	7.15 ± *3.20*	3	10.01 ± *2.07*	3
Core-top		–	–	6.93 ± *3.32*	*1	10.96 ± *2.62*	*1	5.38 ± *0.77*	*1

Note. Sampling intervals and Mg/Ca data. Monthly mean Mg/Ca (mmol/mol) for *G. ruber albus*, *T. clarkei* "big" and "encrusted" of all measurements for the upper four sediment traps. The core top sample was obtained on January 2013 (Steiner et al., 2017). "*n*" marks the number of specimens contributing to the mean, and italic font numbers mark the standard deviation (SD). For samples consisting of one specimen (*n* = 1, labeled with *), the SD was calculated for the measurements of a single specimen. The accompanying supplementary file contains the specimen Mg/Ca and measurement range. Italic values are range.

Thermo Element-2 ICP mass spectrometer (Jochum et al., 2014). Measurements were performed using a 15 Hz pulse repetition rate at low fluence (0.1–0.6 J/cm^2), and 18 s dwelling time. A 30-μm diameter spot size was chosen for analysis as it is the maximum diameter of a single chamber of the small *T. clarkei* (Figure 3). Calibration was performed with the microanalytical synthetic reference material MACS-3 for carbonate, NIST-612, and NIST-610 for calibration as well as NIST-612 for the tuning of the ICP-MS (Jochum et al., 2019). The measurements yielded reproducible results with a relative standard deviation of ~3%–4% for Mg/Ca and Sr/Ca. Single spot measurements were made on each chamber of the individual shells (Figure 3) while verifying the presence of the
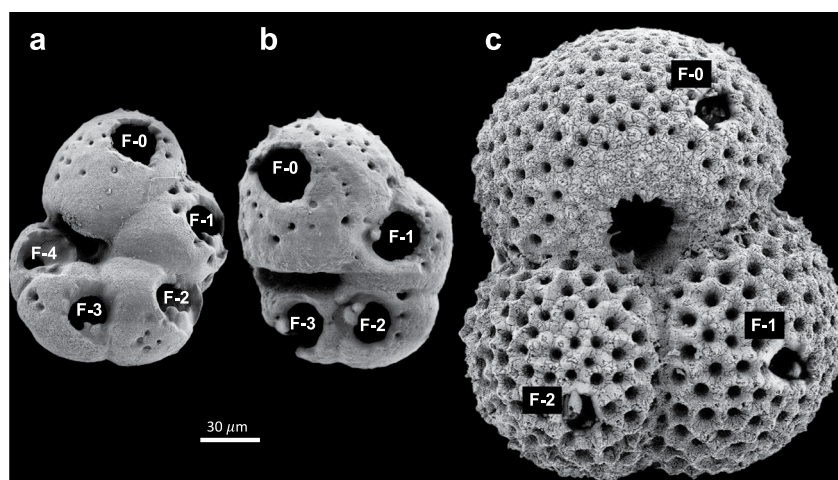
Figure 3. SEM images of PF shells taken from the upper two sediment traps (120 and 220 m) in the GOA. The ablation holes following LA-ICP-MS analyses are evident as large holes. (a) *Turborotalita clarkei* "big" (non-encrusted), (b) *Turborotalita clarkei* "encrusted," and (c) *Globigerinoides ruber albus*. Chambers are labeled F-0 to F-4 from the final to preceding chambers. Additional SEM images can be found in Supporting Information S1 (Figure S7).

spot in the chamber parameters, and not crossing the septae between the chambers. Chambers were named F-0 (final chamber), F-1 (final minus one, i.e., penultimate chamber), F-2, and so on, for the penultimate, antepenultimate, and further chambers, respectively. Average Mg/Ca of single individuals was calculated from all single chamber Mg/Ca data in one shell. The mean Mg/Ca of a specific sampling time-interval was calculated for the upper sediment traps excluding Mg/Ca data from the deepest sediment trap at 570 m given that resuspension of seafloor sediment may have occurred during winter and admixed settled PF shells into the trap (Chernihovsky et al., 2018) (Table 2).

2.4. Scanning Electron Microscopy (SEM)

SEM was used to identify the architecture of the shell wall of 23 specimens of *T. clarkei* (both "big" and "encrusted" morphotypes) and *G. ruber albus* obtained from sediment traps and core top samples. From which, 20 analyzed specimens were obtained from the upper water column (120–220 m water depth intervals) for well-preserved shells of varying Mg/Ca. All samples were coated with gold and analyzed using SEM LEO-1530 at magnification 900x–15000x.

2.5. Statistical Analyses

The mean Mg/Ca of all measurements on PF assemblages of the same species from multiple sediment trap depths (see below for more details) at each given date were calculated and a full description of the specimens Mg/Ca means can be found in Table S1. In *G. ruber albus*, a single outlier measurement was detected where Mg/Ca = 80.52 mmol/mol (April 2015; 120 m water depth interval; chamber F-0). This value is significantly higher than the other measurements (the next highest measurement in *G. ruber albus* yielded Mg/Ca = 19.09). This anomalous value could be related to the lack of oxidative cleaning and/or abnormalities in Mg distribution as it was detected in the last chamber of the specimen (F-0). This outlier was removed from the mean Mg/Ca values in the subsequent analyses.

To account for the temporal difference between the measurement dates of when the oceanographic parameters were measured, and the time-interval of the sediment trap sample, corresponding oceanographic parameter values were calculated using linear interpolation between the dates. The Spearman rank test p-values were calculated to investigate relationships between mean Mg/Ca and data sets of corresponding oceanographic parameters. Furthermore, various non-linear and linear regression models between mean Mg/Ca and oceanographic parameters were calculated and their corresponding coefficients of determination (r^2) were calculated (Figures S2, S3, S4, and S5 in Supporting Information S1). The Mathematica© software was used to calculate the non-linear regressions, based on the "NonlinearModelFit" function, which uses numerical local optimization (Newton method) for parameter estimation. The code is provided with the Supporting Information S1.

3. Results

3.1. Hydrography of the GOA in 2014–2015

During the spring and summer months (April–September) of 2014 and 2015, a thermocline developed in the upper 200 m (Figure 2a, Table 1). The thermocline separated the more nutrient-depleted warm surface waters from the relatively nutrient-replete subsurface layer with a uniform temperature of ~21°C. In the winter/spring of 2014/2015, the thermocline progressively eroded due to surface cooling and a deep mixed surface layer developed, reaching its maximum depth of ~250 m by the end of March 2015. The salinity in the deep-water column was relatively homogenous ca. 40.75, compared with the slightly less saline-mixed layer (Figure 2b, Table 1). The pH values in the GOA ranged between 8.16 and 8.21 in the upper 250 m and between 8.12 and 8.19 beneath the thermocline (Figure 2c, Table 1). The depth distribution of chlorophyll-α varied during the year (Figure 2d), with the highest values in the surface mixed layer during the winter 2014/2015 and spring 2015. A pronounced Deep Chlorophyll Maximum between 60 and 120 m occurred during the 2014 summer months. The oceanographic parameters of the bottom water at ~700 m were relatively stable year-round with a temperature of 21°C, salinity of 40.75, and pH levels of 8.13.

3.2. Mg/Ca and Sr/Ca Variability With Water Depth and Time

The Mg/Ca in *G. ruber albus* exhibits variability between different months but generally remains constant within each depth profile, suggesting that this species calcifies in the mixed layer (Figure 4). This evidence justifies the
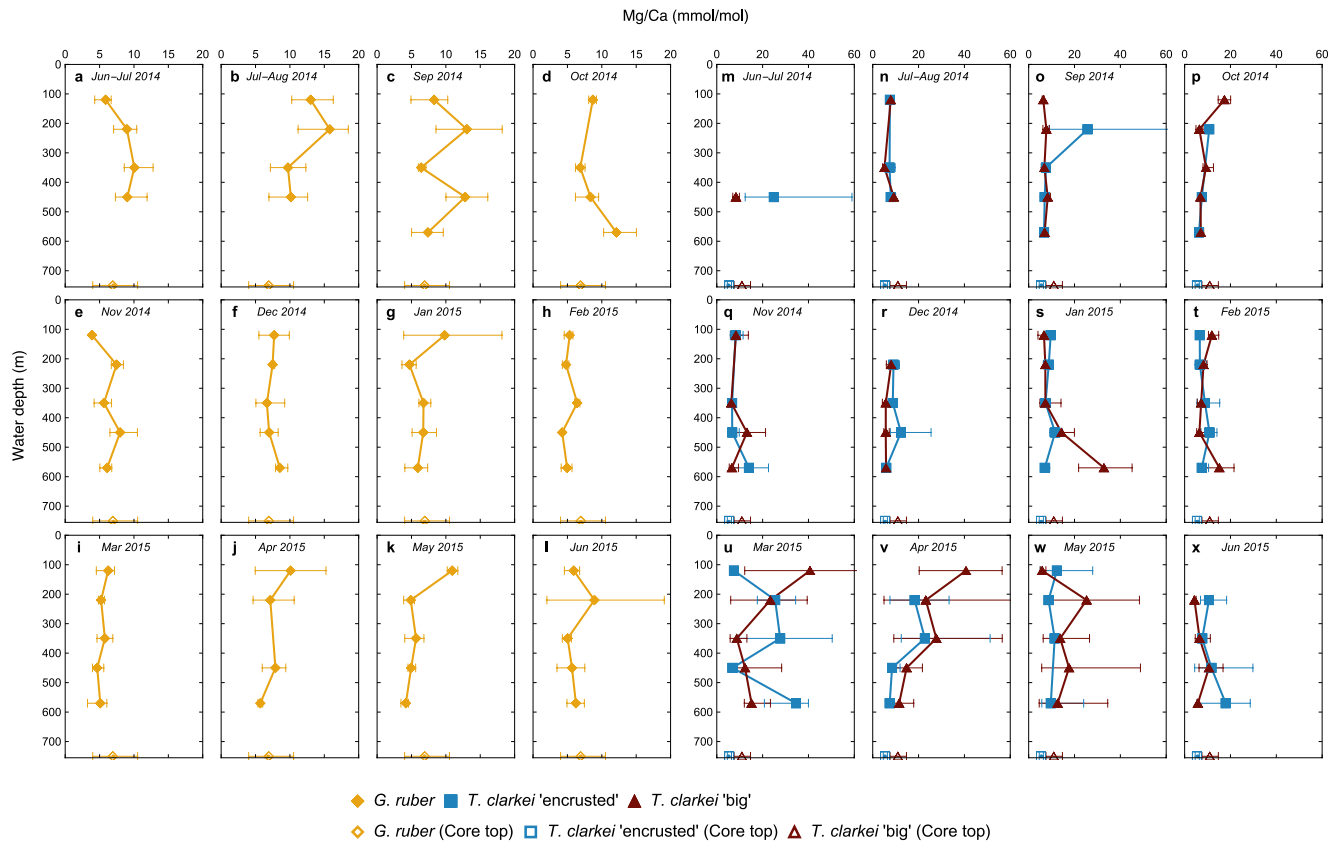
Figure 4. Sediment trap depth profiles of single-specimen's mean Mg/Ca of *G. ruber albus* (a–l), *T. clarkei* "big," and the *T. clarkei* "encrusted" (m–x) shells obtained between June 2014 and June 2015. Values from a core top sample at *Station A* (720 m) are displayed by open symbols on the bottom *x*-axis for comparison. Error bars represent the range (i.e., maxima and minima in the set of measurements for each specimen).

calculation of a mean Mg/Ca for multiple sediment traps at each specific time interval (Table 2). Mean monthly Mg/Ca values of *G. ruber albus* were highest in summertime (peaking during July 2014; Mg/Ca = 12.17 ± 2.83) and subsequently decreased with the progression of the year reaching a minimum during February 2015 (Mg/Ca = 5.20 ± 0.93; Table 2).

Compared to *G. ruber albus*, the profiles of Mg/Ca for *T. clarkei* with its two morphotypes "big" and "encrusted" do not show significant temporal variations in the upper three sampling depth levels 120, 220, and 340 m of the water column, apart from a significantly elevated Mg/Ca in spring time (March and April) (Figure 4; Table 2). During March and April (2015), the Mg/Ca values of *T. clarkei* were 21.28 ± 14.35 and 26.59 ± 10.83 for "big" and 16.86 ± 11.23 and 16.49 ± 7.33 for "encrusted," respectively. Generally, the Mg/Ca is higher for *T. clarkei* throughout the year in comparison to *G. ruber albus*, apart from selected summer months. Based on the error bars in the profiles, it is clear that the Mg/Ca in *G. ruber albus* shows less interchamber variability than the two *T. clarkei* phenotypes. Furthermore, Mg/Ca of the PF shells from the core top are similar to the ratios observed in the sediment traps from the water column (Figure 4, Table 2). In addition to Mg/Ca, the Sr/Ca is approximately 1.5 mmol/mol for *G. ruber albus*, and both types of *T. clarkei* ("big" and "encrusted") and is generally constant with depth and time (Figure S1 in Supporting Information S1).

3.3. Mg/Ca and Shell Structure

SEM analyses were conducted in order to detect differences in shell structure between varying Mg/Ca in the three PF types as well as to detail changes between the two morphotypes *T. clarkei* "big" and "encrusted." SEM analyses of specimens of varying Mg/Ca did not show any differences in their shell structure or signs of overgrowth on the inner or outer side of the shell. Minor signs of dissolution are present in *T. clarkei* "encrusted" specimen on the outer calcite layer. *T. clarkei* "big" exhibits ontogenetic calcite only, while *T. clarkei* "encrusted" displays
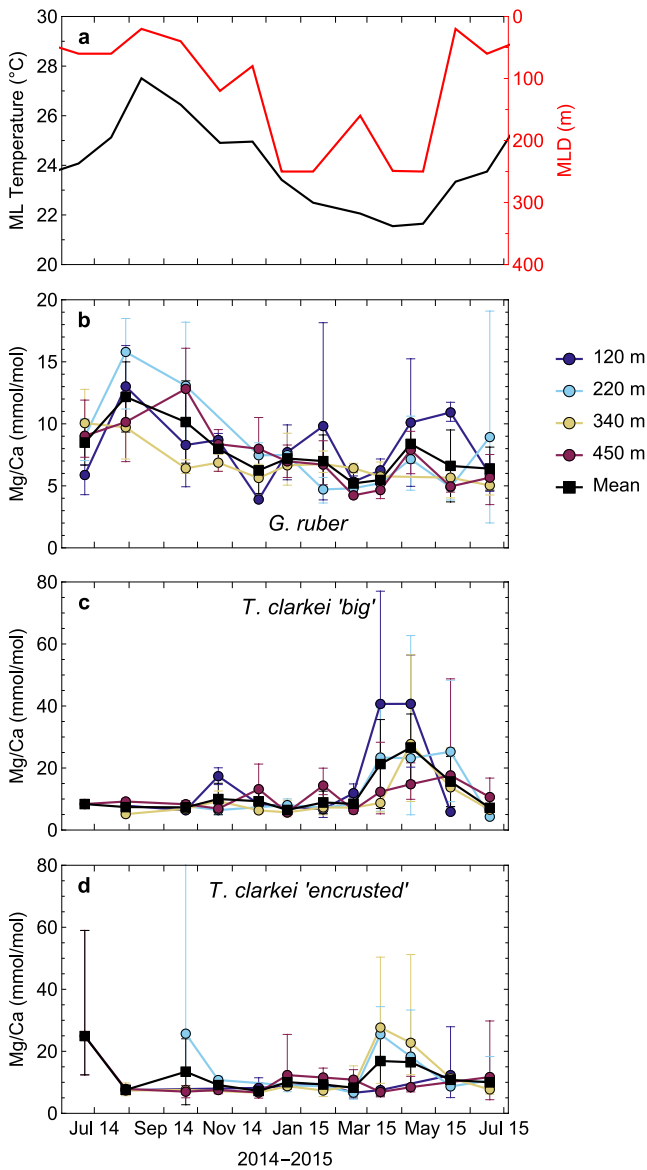
Figure 5. Time series of (a) monthly mixed layer depth (MLD) meters below the surface (red line) and averaged monthly temperatures measured at MLD in situ (black line). (b) *G. ruber albus* Mg/Ca, (c) *T. clarkei* "big" Mg/Ca and (d) *T. clarkei* "encrusted" Mg/Ca. Data points (circles) indicate individual specimens of four upper sediment traps (red, blue, green, and orange). The error bars indicate the measurement range. The black squares represent the mean (and standard deviation) of the four traps for each month.

a systematically thick layer of calcite overgrowth on top of the ontogenetic calcite.

4. Discussion

4.1. Mg/Ca as a Proxy of Hydrology of the GOA

The decreasing Mg/Ca values from the summer to winter (Table 2) provide preliminary evidence that *G. ruber albus* recorded GOA water temperatures. On a time series plot, the various sediment trap depths as well as the mean Mg/Ca of *G. ruber albus* exhibit seasonal temperature trends which follow the mixed layer temperature trends (Figures 5a and 5b). Although *G. ruber albus* is a photosymbiont-bearing species and needs to reside in the sunlit surface mixed layer (Schiebel & Hemleben, 2017), its specific residence depth in the GOA is unknown. Comparing *G. ruber albus* shell Mg/Ca data with calculated mean water temperatures at various fixed water depth intervals between 0 and 120 m yields statistically significant relationships (p-value < 0.05) (Table S2). However, *G. ruber albus* would not likely have resided at one fixed depth interval given the water column mixing in the GOA. The calculated MLD varies significantly over the annual cycle (Schiebel & Hemleben, 2017) and may be assumed to represent the lower residence depth limit for *G. ruber albus* (Figure 5a). Comparing *G. ruber albus* shell Mg/Ca data with the calculated mean temperature in the mixed layer above, the MLD yields the lowest p-value compared to other fixed depth intervals (Table S2).
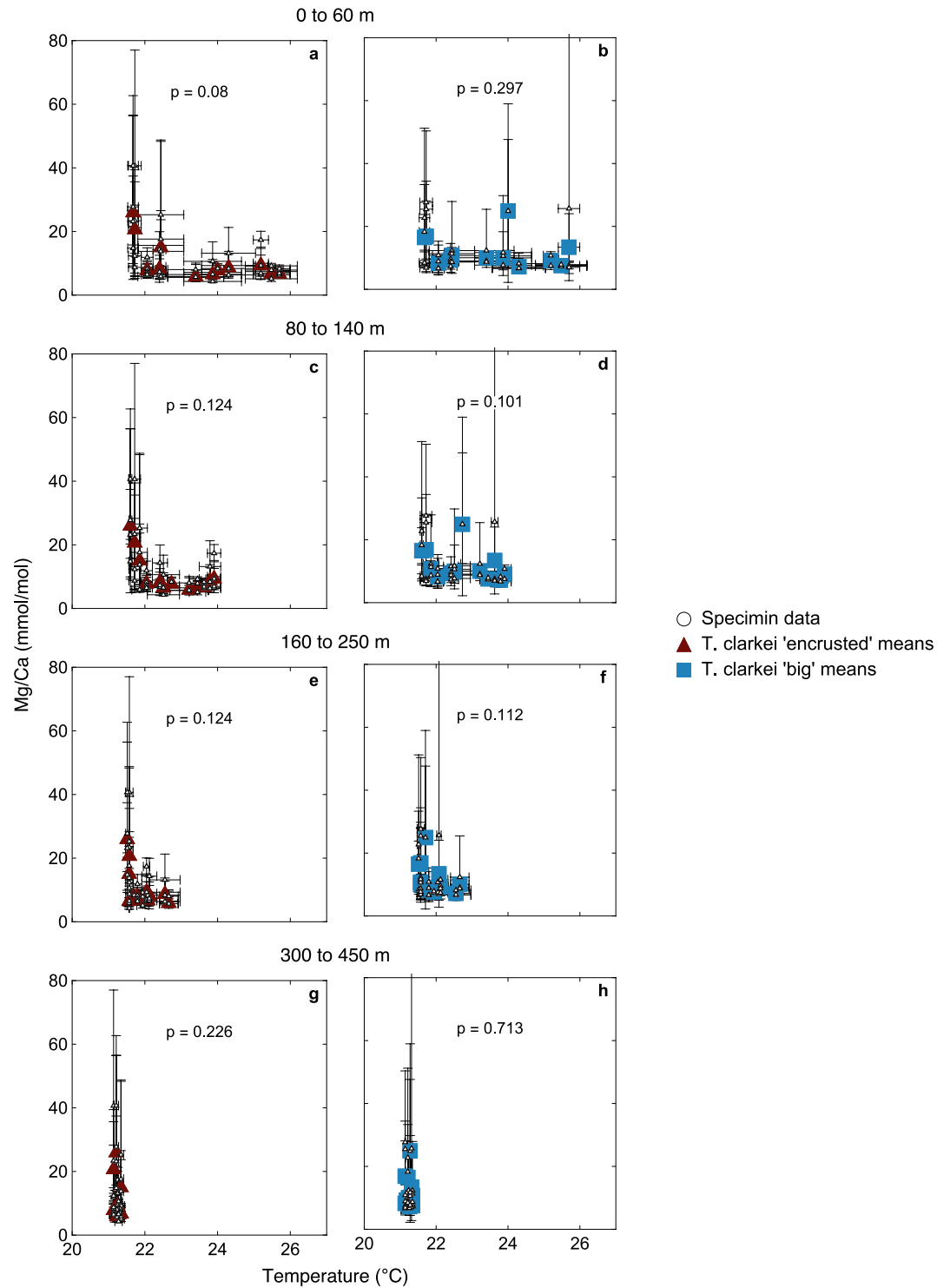
A non-linear exponential regression model is typically used for Mg/Ca-T calibrations in *G. ruber albus* (Equation 1) (Anand et al., 2003; Katz et al., 2010; McConnell & Thunell, 2005):

$$\frac{Mg}{Ca} = B \cdot e^{AT} \tag{1}$$

where T is the calcification temperature, A reflects the Mg/Ca response to a given temperature change, and B is species-specific and related to the environment in which any one species calcifies its shell. When applying the exponential regression model (Equation 1), the resulting r^2 is highest for Mg/Ca versus mean mixed layer temperature (Table S2).

Unlike *G. ruber albus*, there are no previous reports (as far as we know) on the dwelling depth of *T. clarkei*. In fact, the Mg/Ca dynamics and ecology of *T. clarkei* appear to be different than in *G. ruber albus* as illustrated by the significant increase in Mg/Ca values during the late winter and spring (Figures 5c and 5d). Shell calcification in *T. clarkei* may occur below the thermocline, and at increasing water depth with maturation, and is therefore not exposed to strong seasonal temperature changes (Hemleben et al., 1989; Schiebel & Hemleben, 2017). Calculating the *p*-value and regression parameter values of mean Mg/Ca of *T. clarkei* and average temperatures over varying fixed depth interval data sets may provide a clue to their preferred depth habitat (Figure 6). All plots in Figure 6 show *p*-values that are higher than 0.05, suggesting a weak Mg/Ca-T relationship. Both types of *T. clarkei* "big" and "encrusted" exhibit elevated Mg/Ca during the months of maximum water column mixing in March and April (Figure 5c), which are associated with increased phytoplankton production without an increase in ambient water temperature (Figures 2a and 2d). The enriched Mg/Ca in *T. clarkei* shell calcite may have resulted either from the admixture of surface waters at deeper water depth or an ascent of *T. clarkei* up to the deepened surface mixed layer or an effect of alimentation on the Mg/Ca following the phytoplankton bloom.

Figure 6. Mg/Ca of *T. clarkei* "big" (a, c, e, g; monthly mean values are brown triangles; mean specimen are empty circles with range as error bars) and *T. clarkei* "encrusted" (b, d, f, h; mean monthly are blue squares; mean specimen are empty circles with range as error bars) versus mean temperatures over four fixed water depth intervals (0–60 m, 80–140 m, 160–250 m, 300–450 m). *P*-values are shown in each panel.

4.2. Ontogenetic Effect on Mg/Ca

A prominent feature of both *G. ruber albus* and *T. clarkei* in the GOA is the systematically elevated Mg/Ca (>5 mmol/mol) throughout the sampling year. In addition to temperature, factors that might influence the Mg/Ca in the shell calcite include salinity, pH, $[CO_3^{-2}]$, and post-depositional alteration. These effects have been studied extensively in culture experiments and sediment samples at the species level as well as intra-individual (chamber-to-chamber) variations (Allen et al., 2016; Bolton et al., 2011; Brown & Elderfield, 1996; Evans, Wade, et al., 2016; Fehrenbacher et al., 2020; Friedrich et al., 2012; Gibson et al., 2016; Gray et al., 2018; Katz et al., 2010).

G. ruber albus is a symbiont-bearing species which dwells in the sunlit surface mixed layer, usually in the upper 60 m of the water column and does not perform secondary calcification on top of the ontogenetic shell (e.g., Numberger et al., 2009; Wang, 2000). Unlike *G. ruber albus*, *T. clarkei* produces secondary calcite at depth, possibly following reproduction (Bé, 1980; Hamilton et al., 2008; Hemleben et al., 1989). The trace element composition was expected to vary between the "big" and "encrusted" morphotypes (Jonkers et al., 2012). However, no significant differences were detected between their shell-bound Mg/Ca with increasing water depth. Lower Mg/Ca in the shell calcite of *T. clarkei* "encrusted" would be expected if forming any calcite in colder temperatures at depth. Similar observations were made by Mezger et al. (2018) on shell-bound Mg/Ca in shells from core-tops and plankton tows obtained from a North-South transect in the Red Sea.

The shell-bound Mg/Ca is not likely to reflect "vital effects" because the three different types of PF display elevated Mg/Ca. The two *T. clarkei* types may represent different life stages as *T. clarkei* "big" may be considered pre-reproduction and the "encrusted" type (post-) reproduction type, analogous to *Neogloboquadrina pachyderma* (Eggins et al., 2003). In addition, different life strategies can be considered, as *G. ruber albus* is symbiont-bearing and *T. clarkei* is assumed symbiont barren. Furthermore, the dietary preferences of *G. ruber albus* are possibly more carnivorous than those of *T. clarkei*, which is assumed to be a rather detritivorous feeding on the exported matter below the pycnocline (Schiebel & Hemleben, 2017).

## 4.3. Effect of Preservation on Mg/Ca

The preservation of the PF shells, or inversely, the dissolution with increasing water depth that can affect the shell-bound Mg/Ca, can be assessed from Sr/Ca in the shell calcite (Brown & Elderfield, 1996; Elderfield et al., 2000; Fehrenbacher & Martin, 2014; Lea et al., 1999; Regenberg et al., 2006, 2014). Sr/Ca is conservative in seawater on seasonal timescales and is on the same order of magnitude for each species and facilitates an assessment of any biases on the Mg/Ca (and other ME/Ca) and monitoring the quality of the LA-ICP-MS analyses (Friedrich et al., 2012; Kisakürek et al., 2011; Lear et al., 2003; Schiebel & Hemleben, 2017).

G. ruber albus in the GOA yields Sr/Ca ~1.5 mmol/mol, similar to observations from a core top survey from the North Atlantic (Elderfield et al., 2000; Gupta, 1999) (Figure S1 in Supporting Information S1). Furthermore, SEM imaging showed little signs of dissolution in a sample of *T. clarkei* "big" derived from the upper water column, which would be expected to lower the Mg/Ca (Subhas et al., 2018). As the Sr/Ca from the GOA agrees well with the values reported in the literature, any dissolution effects may be considered to be negligible (Cléroux et al., 2008; Elderfield et al., 2000, 2002; Johnstone et al., 2011; Rosenthal & Lohmann, 2002; Rosenthal et al., 2004).

Planktic foraminifer shells from a core-top underlying the sediment trap mooring display the same range of Mg/Ca as PF from the sediment traps and support the idea that the elevated Mg incorporation to the shell-calcite occurs in the water column (Figure 4). However, Hoogakker et al. (2009) suggested that the elevated and non-homogeneous Mg/Ca in the shell calcite is due to secondary elevated Mg-calcite overgrowth that occurred at the water-sediment interface in the Red Sea. This stems from the assumption that interstitial waters supersaturated in $CaCO_3$ may support calcite overgrowth in the interstitial phase (Kisakürek et al., 2008; Lea et al., 1999; Nürnberg et al., 1996). In this study, we did not observe such overgrowth in the lowest and most elevated Mg/Ca individuals using SEM.

4.4. Incorporating Hypersaline Regions in Mg/Ca-T Calibrations

Earlier studies have shown the effect of non-thermal factors on the Mg/Ca in PF such as ontogeny and shell size (Anand & Elderfield, 2005; Anand et al., 2003; Friedrich et al., 2012), species specific and ecological
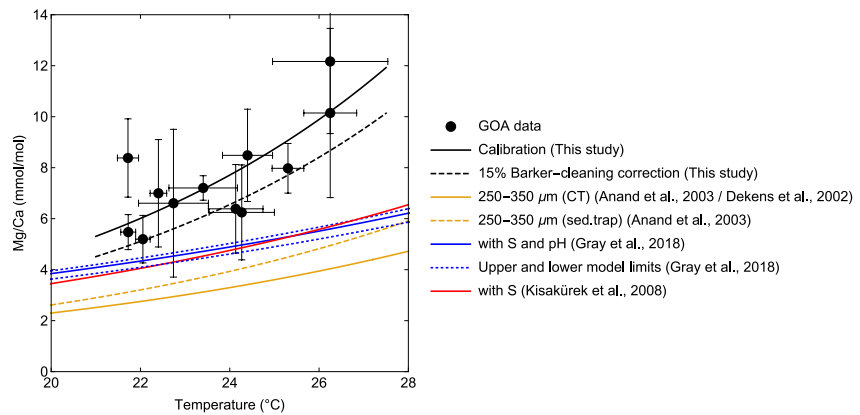
Figure 7. *Globigerinoides ruber albus* Mg/Ca-based temperature calibration model from the GOA using the exponential fit (black curve; Mg/Ca $=0.39 \cdot e^{0.12T}$; $r^2 = 0.975$) and comparison to other temperature calibrations Equations 2 and 3 (orange curves) 5 (red curve) and 6 (green curves). The new results (black squares) represent the average values of all specimens from the upper four sediment traps ($\pm$SD) compared with mixed layer temperatures (error bar = range of temperatures for sediment trap month).

requirements (Anand et al., 2003; Bemis et al., 2002; Cléroux et al., 2008; Friedrich et al., 2012; McConnell & Thunell, 2005), salinity (e.g., Gray et al., 2018; Hoogakker et al., 2009; Kisakürek et al., 2008), and the marine carbonate system (Gray & Evans, 2019; Gray et al., 2018; Russell et al., 2004, and references therein). Saenger and Evans et al. (2019) quantified the effect of non-thermal parameters on the Mg/Ca-T calibration of individual shells of five PF species and showed that the impact of these parameters varies between species. In contrast, Rosenthal et al. (2022) showed that most uni- and multi-variable Mg/Ca-T calibrations reliably reconstruct paleo-temperatures with little differences ($\pm 1°$C) and argued that the Mg/Ca in PF is a robust tracer of ambient seawater temperature regardless of the biases that arise from the non-thermal parameters. Anand et al. (2003) emphasized the effect of shell size and species-specific temperature on Mg/Ca. The Mg/Ca-T calibration of Anand et al. (2003) is based on the exponential fit (Equation 1) for (a) *G. ruber albus* of the 250–350 μm size-fraction from sediment traps (Equation 2), and (b) other species from core tops, except of *Orbulina universa* shells larger than 250 μm (Equation 3):

$$\frac{Mg}{Ca} = 0.34(\pm 0.08) \cdot e^{0.102(\pm 0.01)T} \tag{2}$$

$$\frac{Mg}{Ca} = 0.38 \cdot e^{0.09T} \tag{3}$$

When applying the above annual range of water column temperatures for the GOA using the above calibrations (Equations 2 and 3), the calculated Mg/Ca values are significantly lower than those measured for *G. ruber albus* (Figure 7). The calibrations provided by Anand et al. (2003) do not consider non-thermal parameters such as salinity, which may affect calculated temperatures in both cultured samples and core top samples of *G. ruber albus* by up to 3.3% $\pm$ 1.7% per salinity unit (Gray et al., 2018; Hönisch et al., 2013) or even higher (Arbuszewski et al., 2010; Dueñas-Bohórquez et al., 2009; Evans, Brierley, et al., 2016; Ferguson et al., 2008; Gray & Evans, 2019; Groeneveld et al., 2018; Mathien-Blard & Bassinot, 2009, and references within). High salinity results in elevated shell-bound Mg/Ca and may hamper the use of Mg/Ca as a temperature proxy (Gray et al., 2018; Kısakürek et al., 2008; Lea et al., 1999; Nürnberg et al., 1996). Therefore, we examine two more Mg/Ca calibrations which, in addition to temperature, consider the effect of salinity, pH, and the carbonate system on the uptake of Mg into the shell-calcite (Gray et al., 2018; Kisakürek et al., 2008). Kisakürek et al. (2008) provide a calibration from cultured samples from the GOA applying a salinity control over the Mg/Ca shell-calcite in *G. ruber albus* (Equation 4):

$$\frac{Mg}{Ca} = e^{0.06(\pm 0.02)S+0.08(\pm 0.02)T-2.8(\pm 1.0)} \tag{4}$$
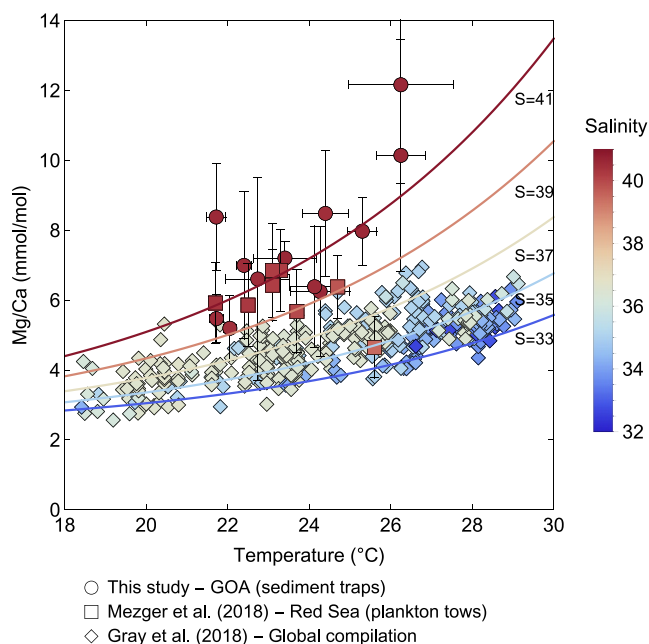
Figure 8. A revised global calibration of Mg/Ca of *G. ruber albus* versus temperature and salinity based on the results of this study (GOA) by Mezger et al. (2018), and the global compilation of Gray et al. (2018).

The calibration provided by Gray et al. (2018) is based on published PF data from 440 sediment trap/plankton tow samples from the Atlantic, Pacific, and Indian oceans, the Bay of Bengal, Arabian Sea, and the tropical Atlantic Ocean. It accounts for pH as the carbonate system controlling parameter (alternatively, $[CO_3^{2-}]$ can be used) and salinity (Equation 5):

$$\frac{Mg}{Ca} = e^{0.060(\pm0.008)T + 0.033(\pm0.022)S - 0.83(\pm0.73) \cdot (pH-8) - 1.07(\pm0.80)} \qquad (5)$$

However, similar to the calibrations provided by Anand et al. (2003), these global calibrations which consider salinity (Equation 4) and pH (Equation 5) still yield respective Mg/Ca values that are significantly lower than the Mg/Ca in *G. ruber albus* measured in the GOA (Figure 7).

4.5. A Framework for Global Mg/Ca-T Calibrations Incorporating High Salinity

The global compilation data set (Equation 5) excludes PF shells from high salinity environments, such as the GOA and the Red Sea (Mezger et al., 2018), and the central and eastern Mediterranean Sea (Boussetta et al., 2011; Ferguson et al., 2008; Sabbatini et al., 2011) (Figure 8). Mg/Ca data from the high salinity (37–40) Red Sea (Mezger et al., 2018) are intermediate between the hypersaline GOA and globally compiled data (Figure 8). We combined the mean Mg/Ca data from the GOA (this study) with results of Mezger et al. (2018) and the larger data set (Gray et al., 2018) and implemented a non-linear regression model (see Supporting Information S1), to produce a global Mg/Ca-T calibration model that considers both large temperature and salinity effects (Equation 6; see curves of equal salinity in Figure 8):

$$\frac{Mg}{Ca} = e^{0.14(\pm0.02)T + 0.15(\pm0.02)S - 7.80(\pm1.59)} + 2.17(\pm0.46) \qquad (6)$$

The global Mg/Ca-T calibration model yields $r^2 = 0.9841$ and p-value < 0.05 ($n = 460$). However, although these results are promising, it is important to stress that most of the data are from ocean waters with salinities close to average to open marine values, and the regressions may be biased as a result. Incorporating more Mg/Ca data from high salinity environments will improve the robustness.

In Gray et al. (2018), pH (or $[CO_3^{2-}]$, depending on the carbonate system controlling parameter) is included in the global calibration. There is strong evidence that pH plays a significant role in controlling Mg/Ca. Combined results from sediment traps and culture studies in the range of pH 7.5–8.5 (Evans, Brierley, et al., 2016; Kisakurek et al., 2008) reveals a clear relationship between Mg/Ca and pH. The pH may potentially also be a factor in the elevated Mg/Ca values seen in the GOA. The study by Gibson et al. (2016) in the eastern equatorial Pacific Ocean reveals elevated values of Mg/Ca in *G. ruber* along with other species. These elevated values could be driven by overgrowth of calcite as shown by SEM images of *Globigerina bulloides* shells together with the relatively low pH (7.6–8.0) of this region. In the GOA, the pH was higher and there was no indication for calcite overgrowth on shells of *G. ruber* and *T. clarkei*. Furthermore, Gibson et al. (2016) found a poor fit between Mg/Ca and Sea Surface Temperature ($r^2 = 0.07$–0.17), albeit with large temperature variations (25°C–32°C). In contrast to our results, which show a very strong fit between Mg/Ca and the MLD temperature ($r^2 = 0.975$; Figure 7).

To illustrate the effect of salinity as opposed to both pH and temperature, we compare data from culture experiment studies by Evans, Brierley, et al. (2016) grown under similar temperature and pH conditions but at lower salinities than the GOA. The GOA data at 26.2°C and a pH of 8.2 yielded Mg/Ca = 10.15 (±3.32) and 12.17 (±2.83) for *G. ruber albus*, while Evans, Brierley, et al. (2016) reported Mg/Ca = 4.99 $\pm$ 0.15 (26°C, and pH = 8.18 $\pm$ 0.01), 4.2 $\pm$ 0.2 (27°C, and pH = 8.13 $\pm$ 0.07), and 3.1 $\pm$ 0.2 (27°C, and pH = 8.29 $\pm$ 0.08). This evidence highlights the role of high salinity in causing the elevated Mg/Ca in the GOA.

Given the apparent strong effect of pH on Mg/Ca, this parameter should be included as an additional parameter into a global Mg/Ca-T calibration. Incorporating Mg/Ca data from high salinity environments with varying pH is

an important future milestone for the global calibration. With the current limited data set, we cannot estimate the effect of pH at high salinities; however, we provide here a framework for the global Mg/Ca-T calibration which accounts for high salinity environments and pH. Using the GOA mean Mg/Ca data and the sediment trap data in Gray et al. (2018), as well as the general equation incorporating T, S, and pH in Gray et al. (2018) (Equation 5), we calculated the following model (Equation 7; $r^2 = 0.9841$):

$$\frac{\text{Mg}}{\text{Ca}} = e^{0.075(\pm0.003)T+0.086(\pm0.007)S+0.034(\pm0.26)\cdot(pH-8)-3.39(\pm0.25)} \tag{7}$$

In the GOA, the mean Mg/Ca in *G. ruber albus* and pH range of 8.17–8.20 reveals a weak positive relationship (Figure S2 in Supporting Information S1). However, this likely reflects the positive relationship observed for temperature and pH in the GOA mixed layer with temperature as the main controlling parameter (Figure S3 in Supporting Information S1). Indeed, taking into account the negative relationship of pH and Mg/Ca and applying the range of pH values that are available in the global calibration of Gray et al. (2018) (7.99–8.12), would result in increased Mg/Ca by 4.2% ± 7.3% and up to 18.6% ± 4.1% (based on pH sensitivities of −8.3% ± 7.3%/0.1 pH and −9.3% ± 4.1%/0.1 pH, respectively; Gray et al., 2018).

The GOA is characterized by a limited high salinity range (~40.4–40.75) in the upper water column and high values relative to the open oceanic settings ranging between 33 and 37 (Zweng et al., 2019). Salinity and shell-bound Mg/Ca of *G. ruber albus* in the GOA show no significant relationship (Figure S4 in Supporting Information S1). The revised global Mg/Ca-T calibration may underestimate the sensitivity of Mg/Ca to salinity given the relatively few points in the high salinity range. Thus, we tested the sensitivity of Mg/Ca to salinity using the data of Figure 8 by plotting Mg/Ca versus salinity at binned temperature intervals (Figure S5 in Supporting Information S1). The salinity sensitivities at all temperature ranges, illustrated as the multiplication factor on salinity in the exponent, are mostly higher than those estimated by Gray et al. (2018), Hönisch et al. (2013), and Kisakürek et al. (2008), and lower than those in Ferguson et al. (2008), Arbuszewski et al. (2010), and Mathien-Blard and Bassinot (2009). It is important to note that the studies mentioning similar or very high sensitivity to salinity were all performed on core top samples from high salinity environments, such as the Eastern Mediterranean and the Red Sea (Arbuszewski et al., 2010; Ferguson et al., 2008; Kisakürek et al., 2008; Mathien-Blard & Bassinot, 2009), while the high sensitivity to salinity in our study stems from in situ observations in the surface water column, that is, the production of the PF shell calcite, and not secondary effects.

Elderfield et al. (2002) showed that the initial D_{Mg} of PF is equivalent to ~0.5 × 10^{-3} and changes linearly with progressing ontogeny. D_{Mg} in benthic foraminifers varies and is affected by factors such as Mg/Ca in seawater, temperature, and salinity, and is characterized by a power fit function or linear correlation (Hauzer et al., 2018, 2021; Le Houedec et al., 2021; Segev & Erez., 2006). We suggest that the D_{Mg} of PF may increase exponentially and not linearly at high salinities (Figure S5 in Supporting Information S1). The hypersaline conditions disproportionately affect Mg uptake into the shell calcite and change the distribution coefficient (D_{Mg}) by allowing for more Mg to be incorporated as well as making it more sensitive to the changing temperatures.

4.6. A Local Mg/Ca-Temperature Calibration

Until more data from other high salinity regions (>38) are available for improving the global calibration, we provide a more accurate local calibration that can be applied to other regions of high salinity similar to the GOA (40–41).

Applying an exponential model fit using *G. ruber albus* mean data of several specimens based on Equation 1, we provide new A and B constants (Equation 8; Figure 7; $r^2 = 0.975$):

$$\frac{\text{Mg}}{\text{Ca}} = 0.39(\pm0.30) \cdot e^{0.12(\pm0.03)T} \tag{8}$$

The local Mg/Ca-T calibration sheds light on the behavior of Mg incorporation into *G. ruber albus* shell calcite in the MLD, a depth interval that has a wide range of temperatures with a more limited range of pH values (8.17–8.20), and a very narrow range of (high) salinities (40.60 ± 0.15). The constants A and B proposed here reflect the unique hydrologic characteristics of the study area, in particular high salinity, and any vital effects that could affect the Mg/Ca as a temperature proxy.

For both the global (Equations 6 and 7) and local calibrations (Equation 8) Mg/Ca data obtained from the lower sediment trap (i.e., 570 m) was excluded to avoid possible biases incurred by the incorporation of resuspended material in the bottom trap, a phenomenon that was observed particularly during winter months (Chernihovsky et al., 2018). In the context of paleo-studies, the sedimentary record documents the integrated water column shell flux and therefore, it can be argued that it is crucial to account for the entire water column (i.e., all sediment traps) and any changes that may affect the Mg/Ca in the shell calcite. Thus, we recalculated and revised global and local calibrations for Mg/Ca data from the upper two sediment traps only (i.e., 120 and 220 m), and, in comparison, from all five sediment traps combined. All models show a good fit between Mg/Ca and mixed layer temperature (Figure S6 in Supporting Information S1; Table S2).

Unlike *G. ruber albus*, the Mg/Ca data for *T. clarkei* in the GOA may not be suitable for paleo-temperature reconstructions. However, Mg/Ca data for *T. clarkei* can potentially be used as a tracer of local water column mixing intensity (Figures 5c and 5d). For example, assuming that the depth of the seasonal mixing is proportional to the intensity of the spring bloom, sharp increases in Mg/Ca in *T. clarkei* in the sedimentary record may be used to investigate past phytoplankton blooms in the GOA as well as serve as marker events in the stratigraphic section.

5. Conclusions

The Mg/Ca of *G. ruber albus* and *T. clarkei* were analyzed on shells from monthly resolved time series sediment traps in the high salinity (~40.5) oligotrophic GOA and assessed for their application as temperature proxies in comparable hypersaline environments. The Mg/Ca in GOA *G. ruber albus* and *T. clarkei* range between 5 and 24 mmol/mol, which is far above average open marine Mg/Ca. Consequently, the existing Mg/Ca-Temperature equations, which are based on average open ocean salinities between 33 and 37, yield unrealistically high calcification temperatures for the PF shells from the GOA. Therefore, a global Mg/Ca-T calibration framework for *G. ruber albus* is proposed, which incorporates a large range of salinities up to 41 (a) and *p*H (b). Additionally, we propose a new local Mg/Ca-T calibration for *G. ruber albus* in the hypersaline GOA (c):

1. $\frac{Mg}{Ca} = e^{0.14(\pm 0.02)T + 0.15(\pm 0.02)S - 7.80(\pm 1.59)} + 2.17(\pm 0.46)$
2. $\frac{Mg}{Ca} = e^{0.075(\pm 0.003)T + 0.086(\pm 0.007)S + 0.034(\pm 0.26) \cdot (pH - 8) - 3.39(\pm 0.25)}$
3. $\frac{Mg}{Ca} = 0.39(\pm 0.30) \cdot e^{0.12(\pm 0.03)T}$

Comparing Mg/Ca in surface dwelling *G. ruber albus* and subsurface dwelling *T. clarkei* may provide information on the hydrological characteristics of past oceans such as temperature difference between the surface and sub-thermocline water column, and stratification of the surface water column, and may be used to infer on nutrient entrainment, trophic conditions, and primary productivity.

Data Availability Statement

Tabular supplementary data generated in this study can be found at PANGAEA (Levy, 2023a). Additional tabular supplementary data and supplementary code can be downloaded from the MPG-repository Edmond (Levy, 2023b).

References

Allen, K. A., Hönisch, B., Eggins, S. M., Haynes, L. L., Rosenthal, Y., & Yu, J. (2016). Trace element proxies for surface ocean conditions: A synthesis of culture calibrations with planktic foraminifera. *Geochimica et Cosmochimica Acta*, *193*, 197–221. https://doi.org/10.1016/j.gca.2016.08.015

Anand, P., & Elderfield, H. (2005). Variability of Mg/Ca and Sr/Ca between and within the planktonic foraminifers *Globigerina bulloides* and *Globorotalia truncatulinoides*. *Geochemistry, Geophysics, Geosystems*, *6*(11), Q11D15. https://doi.org/10.1029/2004gc000811

Anand, P., Elderfield, H., & Conte, M. H. (2003). Calibration of Mg/Ca thermometry in planktonic foraminifera from a sediment trap time series. *Paleoceanography*, *18*(2). https://doi.org/10.1029/2002pa000846

Arbuszewski, J., de Menocal, P., Kaplan, A., & Farmer, E. C. (2010). On the fidelity of shell-derived δ18O seawater estimates. *Earth and Planetary Science Letters*, *300*(3–4), 185–196. https://doi.org/10.1016/j.epsl.2010.10.035

Bé, A. W. H. (1980). Gametogenic calcification in a spinose planktonic foraminifer, *Globigerinoides sacculifer* (Brady). *Marine Micropaleontology*, *5*, 283–310. https://doi.org/10.1016/0377-8398(80)90014-6

Bemis, B. E., Spero, H. J., & Thunell, R. C. (2002). Using species-specific paleotemperature equations with foraminifera: A case study in the Southern California Bight. *Marine Micropaleontology*, *46*(3–4), 405–430. https://doi.org/10.1016/s0377-8398(02)00083-x

Benaltabet, T., Lapid, G., & Torfstein, A. (2020). Seawater Pb concentration and isotopic composition response to daily time scale dust storms in the Gulf of Aqaba, Red Sea. *Marine Chemistry*, *227*, 103895. https://doi.org/10.1016/j.marchem.2020.103895

Berggren, W. A., Kent, D. V., Swisher, C. C., & Aubry, M. P. (1995). A revised Cenozoic geochronology and chronostratigraphy.

Bijma, J., Faber, W. W., & Hemleben, C. (1990). Temperature and salinity limits for growth and survival of some planktonic foraminifers in laboratory cultures. *Journal of Foraminiferal Research*, *20*(2), 95–116. https://doi.org/10.2113/gsjfr.20.2.95

Bijma, J., Hönisch, B., & Zeebe, R. (2002). Impact of the ocean carbonate chemistry on living foraminiferal shell weight: Comment on"Carbonate ion concentration in glacial-age deep waters of the Caribbean Sea" by WS Broecker and E. Clark. *Geochemistry, Geophysics, Geosystems*, *3*(11), 1064–1067. https://doi.org/10.1029/2002gc000388

Biton, E., & Gildor, H. (2011). Stepwise seasonal restratification and the evolution of salinity minimum in the Gulf of Aqaba (Gulf of Eilat). *Journal of Geophysical Research*, *116*(C8), C08022. https://doi.org/10.1029/2011jc007106

Bolton, A., Baker, J. A., Dunbar, G. B., Carter, L., Smith, E. G., & Neil, H. L. (2011). Environmental versus biological controls on Mg/Ca variability in Globigerinoides ruber (white) from core top and plankton tow samples in the southwest Pacific Ocean. *Paleoceanography*, *26*(2). https://doi.org/10.1029/2010pa001924

Boltovskoy, E. (1991). Globigerinita clarkei (Rögl & Bolli)—An unfairly ignored small planktic foraminifer. *Boreas*, *20*(2), 151–154. https://doi.org/10.1111/j.1502-3885.1991.tb00303.x

Boussetta, S., Bassinot, F., Sabbatini, A., Caillon, N., Nouet, J., Kallel, N., et al. (2011). Diagenetic Mg-rich calcite in Mediterranean sediments: Quantification and impact on foraminiferal Mg/Ca thermometry. *Marine Geology*, *280*(1–4), 195–204. https://doi.org/10.1016/j.margeo.2010.12.011

Broecker, W. S., & Clark, E. (1999). CaCO$_3$ size distribution: A paleocarbonate ion proxy? *Paleoceanography*, *14*(5), 596–604. https://doi.org/10.1029/1999pa900016

Brown, S. J., & Elderfield, H. (1996). Variations in Mg/Ca and Sr/Ca ratios of planktonic foraminifera caused by postdepositional dissolution: Evidence of shallow Mg-dependent dissolution. *Paleoceanography*, *11*(5), 543–551. https://doi.org/10.1029/96pa01491

Brummer, G. J. A., Hemleben, C., & Spindler, M. (1986). Planktonic foraminiferal ontogeny and new perspectives for micropalaeontology. *Nature*, *319*(6048), 50–52. https://doi.org/10.1038/319050a0

Chase, Z., Paytan, A., Beck, A., Biller, D., Bruland, K., Measures, C., & Sañudo-Wilhelmy, S. (2011). Evaluating the impact of atmospheric deposition on dissolved trace-metals in the Gulf of Aqaba, Red Sea. *Marine Chemistry*, *126*(1–4), 256–268. https://doi.org/10.1016/j.marchem.2011.06.005

Chen, Y., Paytan, A., Chase, Z., Measures, C., Beck, A. J., Sañudo-Wilhelmy, S. A., & Post, A. F. (2008). Sources and fluxes of atmospheric trace elements to the Gulf of Aqaba, Red Sea. *Journal of Geophysical Research*, *113*(D5), D05306. https://doi.org/10.1029/2007jd009110

Chernihovsky, N., Torfstein, A., & Almogi-Labin, A. (2018). Seasonal flux patterns of planktonic foraminifera in a deep, oligotrophic, marginal sea: Sediment trap time series from the Gulf of Aqaba, northern Red Sea. *Deep Sea Research Part I: Oceanographic Research Papers*, *140*, 78–94. https://doi.org/10.1016/j.dsr.2018.08.003

Cléroux, C., Cortijo, E., Anand, P., Labeyrie, L., Bassinot, F., Caillon, N., & Duplessy, J. C. (2008). Mg/Ca and Sr/Ca ratios in planktonic foraminifera: Proxies for upper water column temperature reconstruction. *Paleoceanography*, *23*(3). https://doi.org/10.1029/2007pa001505

Dissard, D., Nehrke, G., Reichart, G. J., & Bijma, J. (2010). The impact of salinity on the Mg/Ca and Sr/Ca ratio in the benthic foraminifera Ammonia tepida: Results from culture experiments. *Geochimica et Cosmochimica Acta*, *74*(3), 928–940. https://doi.org/10.1016/j.gca.2009.10.040

Dueñas-Bohórquez, A., da Rocha, R. E., Kuroyanagi, A., Bijma, J., & Reichart, G. J. (2009). Effect of salinity and seawater calcite saturation state on Mg and Sr incorporation in cultured planktonic foraminifera. *Marine Micropaleontology*, *73*(3–4), 178–189. https://doi.org/10.1016/j.marmicro.2009.09.002

Eggins, S., De Deckker, P., & Marshall, J. (2003). Mg/Ca variation in planktonic foraminifera tests: Implications for reconstructing palaeo-seawater temperature and habitat migration. *Earth and Planetary Science Letters*, *212*(3–4), 291–306. https://doi.org/10.1016/s0012-821x(03)00283-8

Elderfield, H., Cooper, M., & Ganssen, G. (2000). Sr/Ca in multiple species of planktonic foraminifera: Implications for reconstructions of seawater Sr/Ca. *Geochemistry, Geophysics, Geosystems*, *1*(11), 1017. https://doi.org/10.1029/1999gc000031

Elderfield, H., & Ganssen, G. (2000). Past temperature and δ^{18}O of surface ocean waters inferred from foraminiferal Mg/Ca ratios. *Nature*, *405*(6785), 442–445. https://doi.org/10.1038/35013033

Elderfield, H., Vautravers, M., & Cooper, M. (2002). The relationship between shell size and Mg/Ca, Sr/Ca, δ^{18}O, and δ^{13}C of species of planktonic foraminifera. *Geochemistry, Geophysics, Geosystems*, *3*(8), 1–13. https://doi.org/10.1029/2001gc000194

Evans, D., Brierley, C., Raymo, M. E., Erez, J., & Müller, W. (2016). Planktic foraminifera shell chemistry response to seawater chemistry: Pliocene–Pleistocene seawater Mg/Ca, temperature and sea level change. *Earth and Planetary Science Letters*, *438*, 139–148. https://doi.org/10.1016/j.epsl.2016.01.013

Evans, D., Sagoo, N., Renema, W., Cotton, L. J., Müller, W., Todd, J. A., et al. (2018). Eocene greenhouse climate revealed by coupled clumped isotope-Mg/Ca thermometry. *Proceedings of the National Academy of Sciences of the United States of America*, *115*(6), 1174–1179. https://doi.org/10.1073/pnas.1714744115

Evans, D., Wade, B. S., Henehan, M., Erez, J., & Müller, W. (2016). Revisiting carbonate chemistry controls on planktic foraminifera Mg/Ca: Implications for sea surface temperature and hydrology shifts over the Paleocene–Eocene thermal maximum and Eocene–Oligocene transition. *Climate of the Past*, *12*(4), 819–835. https://doi.org/10.5194/cp-12-819-2016

Fehrenbacher, J., Marchitto, T., & Spero, H. J. (2020). Comparison of laser ablation and solution-based ICP-MS results for individual foraminifer Mg/Ca and Sr/Ca analyses. *Geochemistry, Geophysics, Geosystems*, *21*(12), e2020GC009254. https://doi.org/10.1029/2020gc009254

Fehrenbacher, J. S., & Martin, P. A. (2014). Exploring the dissolution effect on the intrashell Mg/Ca variability of the planktic foraminifer *Globigerinoides ruber*. *Paleoceanography*, *29*(9), 854–868. https://doi.org/10.1002/2013pa002571

Ferguson, J. E., Henderson, G. M., Kucera, M., & Rickaby, R. E. M. (2008). Systematic change of foraminiferal Mg/Ca ratios across a strong salinity gradient. *Earth and Planetary Science Letters*, *265*(1–2), 153–166. https://doi.org/10.1016/j.epsl.2007.10.011

Friedrich, O., Schiebel, R., Wilson, P. A., Weldeab, S., Beer, C. J., Cooper, M. J., & Fiebig, J. (2012). Influence of test size, water depth, and ecology on Mg/Ca, Sr/Ca, δ^{18}O, and δ^{13}C in nine modern species of planktic foraminifers. *Earth and Planetary Science Letters*, *319*, 133–145. https://doi.org/10.1016/j.epsl.2011.12.002

Ganor, E., & Foner, H. A. (2001). Mineral dust concentrations, deposition fluxes and deposition velocities in dust episodes over Israel. *Journal of Geophysical Research*, *106*(D16), 18431–18437. https://doi.org/10.1029/2000jd900535

Gibson, K. A., Thunell, R. C., Machain-Castillo, M. L., Fehrenbacher, J., Spero, H. J., Wejnert, K., et al. (2016). Evaluating controls on planktonic foraminiferal geochemistry in the Eastern Tropical North Pacific. *Earth and Planetary Science Letters*, *452*, 90–103. https://doi.org/10.1016/j.epsl.2016.07.039

Gray, W. R., & Evans, D. (2019). Nonthermal influences on Mg/Ca in planktonic foraminifera: A review of culture studies and application to the last glacial maximum. *Paleoceanography and Paleoclimatology*, *34*(3), 306–315. https://doi.org/10.1029/2018pa003517

Gray, W. R., Weldeab, S., Lea, D. W., Rosenthal, Y., Gruber, N., Donner, B., & Fischer, G. (2018). The effects of temperature, salinity, and the carbonate system on Mg/Ca in *Globigerinoides ruber* (white): A global sediment trap calibration. *Earth and Planetary Science Letters*, *482*, 607–620. https://doi.org/10.1016/j.epsl.2017.11.026

Groeneveld, J., Filipsson, H. L., Austin, W. E., Darling, K., McCarthy, D., Quintana Krupinski, N. B., et al. (2018). Assessing proxy signatures of temperature, salinity, and hypoxia in the Baltic Sea through foraminifera-based geochemistry and faunal assemblages. *Journal of Micropalaeontology*, *37*(2), 403–429. https://doi.org/10.5194/jm-37-403-2018

Gupta, B. K. S. (1999). In B. K. S. Gupta (Ed.), *Modern foraminifera* (pp. 7–36). Kluwer Academic Publishers.

Hamilton, C. P., Spero, H. J., Bijma, J., & Lea, D. W. (2008). Geochemical investigation of gametogenic calcite addition in the planktonic foraminifera *Orbulina universa*. *Marine Micropaleontology*, *68*(3–4), 256–267. https://doi.org/10.1016/j.marmicro.2008.04.003

Hastings, D. W., Russell, A. D., & Emerson, S. R. (1998). Foraminiferal magnesium in *Globeriginoides sacculifer* as a paleotemperature proxy. *Paleoceanography*, *13*(2), 161–169. https://doi.org/10.1029/97pa03147

Hauzer, H., Evans, D., Müller, W., Rosenthal, Y., & Erez, J. (2018). Calibration of Na partitioning in the calcitic foraminifer *Operculina ammonoides* under variable Ca concentration: Toward reconstructing past seawater composition. *Earth and Planetary Science Letters*, *497*, 80–91. https://doi.org/10.1016/j.epsl.2018.06.004

Hauzer, H., Evans, D., Müller, W., Rosenthal, Y., & Erez, J. (2021). Salinity effect on trace element incorporation in cultured shells of the large benthic foraminifer *Operculina ammonoides*. *Paleoceanography and Paleoclimatology*, *36*(6), e2021PA004218. https://doi.org/10.1029/2021pa004218

Hemleben, C., Spindler, M., & Anderson, O. R. (1989). Taxonomy and species features. In *Modern planktonic foraminifera* (pp. 8–32). Springer.

Hönisch, B., Allen, K. A., Lea, D. W., Spero, H. J., Eggins, S. M., Arbuszewski, J., et al. (2013). The influence of salinity on Mg/Ca in planktic foraminifers–Evidence from cultures, core-top sediments and complementary $\delta_{18}O$. *Geochimica et Cosmochimica Acta*, *121*, 196–213. https://doi.org/10.1016/j.gca.2013.07.028

Hoogakker, B. A., Klinkhammer, G. P., Elderfield, H., Rohling, E. J., & Hayward, C. (2009). Mg/Ca paleothermometry in high salinity environments. *Earth and Planetary Science Letters*, *284*(3–4), 583–589. https://doi.org/10.1016/j.epsl.2009.05.027

Jochum, K. P., Jentzen, A., Schiebel, R., Stoll, B., Weis, U., Leitner, J., et al. (2019). High-resolution Mg/Ca measurements of foraminifer shells using femtosecond LA-ICP-MS for paleoclimate proxy development. *Geochemistry, Geophysics, Geosystems*, *20*(4), 2053–2063. https://doi.org/10.1029/2018gc008091

Jochum, K. P., Stoll, B., Weis, U., Jacob, D. E., Mertz-Kraus, R., & Andreae, M. O. (2014). Non-matrix-matched calibration for the multi-element analysis of geological and environmental samples using 200 nm femtosecond LA-ICP-MS: A comparison with nanosecond lasers. *Geostandards and Geoanalytical Research*, *38*(3), 265–292. https://doi.org/10.1111/j.1751-908x.2014.12028.x

Johnstone, H. J., Yu, J., Elderfield, H., & Schulz, M. (2011). Improving temperature estimates derived from Mg/Ca of planktonic foraminifera using X-ray computed tomography–based dissolution index, XDX. *Paleoceanography*, *26*(1). https://doi.org/10.1029/2009pa001902

Jonkers, L., De Nooijer, L. J., Reichart, G. J., Zahn, R., & Brummer, G. J. (2012). Encrustation and trace element composition of *Neogloboquadrina dutertrei* assessed from single chamber analyses–implications for paleotemperature estimates. *Biogeosciences*, *9*(11), 4851–4860. https://doi.org/10.5194/bg-9-4851-2012

Katz, M. E., Cramer, B. S., Franzese, A., Hönisch, B., Miller, K. G., Rosenthal, Y., & Wright, J. D. (2010). Traditional and emerging geochemical proxies in foraminifera. *Journal of Foraminiferal Research*, *40*(2), 165–192. https://doi.org/10.2113/gsjfr.40.2.165

Katz, T., Ginat, H., Eyal, G., Steiner, Z., Braun, Y., Shalev, S., & Goodman-Tchernov, B. N. (2015). Desert flash floods form hyperpycnal flows in the coral-rich Gulf of Aqaba, Red Sea. *Earth and Planetary Science Letters*, *417*, 87–98. https://doi.org/10.1016/j.epsl.2015.02.025

Kısakürek, B., Eisenhauer, A., Böhm, F., Garbe-Schönberg, D., & Erez, J. (2008). Controls on shell Mg/Ca and Sr/Ca in cultured planktonic foraminiferan, *Globigerinoides ruber* (white). *Earth and Planetary Science Letters*, *273*(3–4), 260–269. https://doi.org/10.1016/j.epsl.2008.06.026

Kısakürek, B., Eisenhauer, A., Böhm, F., Hathorne, E. C., & Erez, J. (2011). Controls on calcium isotope fractionation in cultured planktic foraminifera, *Globigerinoides ruber* and *Globigerinella siphonifera*. *Geochimica et Cosmochimica Acta*, *75*(2), 427–443. https://doi.org/10.1016/j.gca.2010.10.015

Kucera, M. (2007). Chapter six planktonic foraminifera as tracers of past oceanic environments. *Developments in Marine Geology*, *1*, 213–262.

Lazar, B., Erez, J., Silverman, J., Rivlin, T., Rivlin, A., Dray, M., et al. (2008). Recent environmental changes in the chemical-biological oceanography of the Gulf of Aqaba (Eilat). *Aqaba-Eilat, the Improbable Gulf. Environment, Biodiversity and Preservation*, 49–61.

Lea, D. W. (1999). Trace elements in foraminiferal calcite. In *Modern foraminifera* (pp. 259–277). Springer.

Lea, D. W., Mashiotta, T. A., & Spero, H. J. (1999). Controls on magnesium and strontium uptake in planktonic foraminifera determined by live culturing. *Geochimica et Cosmochimica Acta*, *63*(16), 2369–2379. https://doi.org/10.1016/s0016-7037(99)00197-0

Lear, C. H., Elderfield, H., & Wilson, P. A. (2003). A Cenozoic seawater Sr/Ca record from benthic foraminiferal calcite and its application in determining global weathering fluxes. *Earth and Planetary Science Letters*, *208*(1–2), 69–84. https://doi.org/10.1016/s0012-821x(02)01156-1

Le Houedec, S., Erez, J., & Rosenthal, Y. (2021). Testing the influence of changing seawater Ca concentration on elements/Ca ratios in planktic foraminifera: A culture experiment. *Geochemistry, Geophysics, Geosystems*, *22*(3), e2020GC009496. https://doi.org/10.1029/2020gc009496

Levy, N. (2023a). Mg/Ca of *Globigerinoides ruber albus* and *Turborotalita clarkei* from water column and core top samples in the hypersaline Gulf of Aqaba [Dataset]. PANGAEA. https://doi.org/10.1594/PANGAEA.959629

Levy, N. (2023b). Temperature calibration of elevated Mg/Ca in planktic Foraminifera shells from the hypersaline Gulf of Aqaba. V1 [Dataset]. https://doi.org/10.17617/3.EXFQC2

Mathien-Blard, E., & Bassinot, F. (2009). Salinity bias on the foraminifera Mg/Ca thermometry: Correction procedure and implications for past ocean hydrographic reconstructions. *Geochemistry, Geophysics, Geosystems*, *10*(12), Q12011. https://doi.org/10.1029/2008gc002353

McConnell, M. C., & Thunell, R. C. (2005). Calibration of the planktonic foraminiferal Mg/Ca paleothermometer: Sediment trap results from the Guaymas Basin, Gulf of California. *Paleoceanography*, *20*(2). https://doi.org/10.1029/2004pa001077

Meeder, E., Mackey, K. R., Paytan, A., Shaked, Y., Iluz, D., Stambler, N., et al. (2012). Nitrite dynamics in the open ocean clues from seasonal and diurnal variations. *Marine Ecology Progress Series*, *453*, 11–26. https://doi.org/10.3354/meps09525

Mezger, E. M., de Nooijer, L. J., Siccha, M., Brummer, G. J., Kucera, M., & Reichart, G. J. (2018). Taphonomic and ontogenetic effects on Na/Ca and Mg/Ca in spinose planktonic foraminifera from the Red Sea. *Geochemistry, Geophysics, Geosystems*, *19*(11), 4174–4194. https://doi.org/10.1029/2018gc007852

Morard, R., Füllberg, A., Brummer, G. J. A., Greco, M., Jonkers, L., Wizemann, A., et al. (2019). Genetic and morphological divergence in the warm-water planktonic foraminifera genus Globigerinoides. *PLoS One*, *14*(12), e0225246. https://doi.org/10.1371/journal.pone.0225246

Mortyn, P. G., & Martínez-Botí, M. A. (2007). Planktonic foraminifera and their proxies for the reconstruction of surface-ocean climate parameters. *Contributions In Science*, 371–383.

Numberger, L., Hemleben, C., Hoffmann, R., Mackensen, A., Schulz, H., Wunderlich, J. M., & Kucera, M. (2009). Habitats, abundance patterns and isotopic signals of morphotypes of the planktonic foraminifer *Globigerinoides ruber* (d'Orbigny) in the eastern Mediterranean Sea since the Marine Isotopic Stage 12. *Marine Micropaleontology*, *73*(1–2), 90–104. https://doi.org/10.1016/j.marmicro.2009.07.004

Nürnberg, D., Bijma, J., & Hemleben, C. (1996). Assessing the reliability of magnesium in foraminiferal calcite as a proxy for water mass temperatures. *Geochimica et Cosmochimica Acta*, *60*(5), 803–814. https://doi.org/10.1016/0016-7037(95)00446-7

O'Brien, C. L., Foster, G. L., Martínez-Botí, M. A., Abell, R., Rae, J. W., & Pancost, R. D. (2014). High sea surface temperatures in tropical warm pools during the Pliocene. *Nature Geoscience*, *7*(8), 606–611. https://doi.org/10.1038/ngeo2194

Paytan, A., Mackey, K. R., Chen, Y., Lima, I. D., Doney, S. C., Mahowald, N., et al. (2009). Toxicity of atmospheric aerosols on marine phytoplankton. *Proceedings of the National Academy of Sciences of the United States of America*, *106*(12), 4601–4605. https://doi.org/10.1073/pnas.0811486106

Regenberg, M., Nürnberg, D., Steph, S., Groeneveld, J., Garbe-Schönberg, D., Tiedemann, R., & Dullo, W. C. (2006). Assessing the effect of dissolution on planktonic foraminiferal Mg/Ca ratios: Evidence from Caribbean core tops. *Geochemistry, Geophysics, Geosystems*, *7*(7), Q07P15. https://doi.org/10.1029/2005gc001019

Regenberg, M., Regenberg, A., Garbe-Schönberg, D., & Lea, D. W. (2014). Global dissolution effects on planktonic foraminiferal Mg/Ca ratios controlled by the calcite-saturation state of bottom waters. *Paleoceanography*, *29*(3), 127–142. https://doi.org/10.1002/2013pa002492

Reiss, Z., & Hottinger, L. (1984). 150,000 years Gulf of Aqaba. In *The Gulf of Aqaba* (pp. 285–319). Springer.

Rosenthal, Y. (2007). Chapter nineteen elemental proxies for reconstructing Cenozoic seawater paleotemperatures from calcareous fossils. *Developments in Marine Geology*, *1*, 765–797.

Rosenthal, Y., Bova, S., & Zhou, X. (2022). A user guide for choosing planktic foraminiferal Mg/Ca-temperature calibrations. *Paleoceanography and Paleoclimatology*, *37*(6), e2022PA004413. https://doi.org/10.1029/2022pa004413

Rosenthal, Y., Boyle, E. A., & Slowey, N. (1997). Temperature control on the incorporation of magnesium, strontium, fluorine, and cadmium into benthic foraminiferal shells from Little Bahama Bank: Prospects for thermocline paleoceanography. *Geochimica et Cosmochimica Acta*, *61*(17), 3633–3643. https://doi.org/10.1016/s0016-7037(97)00181-6

Rosenthal, Y., & Lohmann, G. P. (2002). Accurate estimation of sea surface temperatures using dissolution-corrected calibrations for Mg/Ca paleothermometry. *Paleoceanography*, *17*(3), 16–21. https://doi.org/10.1029/2001pa000749

Rosenthal, Y., Perron-Cashman, S., Lear, C. H., Bard, E., Barker, S., Billups, K., et al. (2004). Interlaboratory comparison study of Mg/Ca and Sr/Ca measurements in planktonic foraminifera for paleoceanographic research. *Geochemistry, Geophysics, Geosystems*, *5*(4), Q04D09. https://doi.org/10.1029/2003gc000650

Russell, A. D., Hönisch, B., Spero, H. J., & Lea, D. W. (2004). Effects of seawater carbonate ion concentration and temperature on shell U, Mg, and Sr in cultured planktonic foraminifera. *Geochimica et Cosmochimica Acta*, *68*(21), 4347–4361. https://doi.org/10.1016/j.gca.2004.03.013

Sabbatini, A., Bassinot, F., Boussetta, S., Negri, A., Rebaubier, H., Dewilde, F., et al. (2011). Further constraints on the diagenetic influences and salinity effect on *Globigerinoides ruber* (white) Mg/Ca thermometry: Implications in the Mediterranean Sea. *Geochemistry, Geophysics, Geosystems*, *12*(10), Q10005. https://doi.org/10.1029/2011gc003675

Sadekov, A., Eggins, S. M., De Deckker, P., Ninnemann, U., Kuhnt, W., & Bassinot, F. (2009). Surface and subsurface seawater temperature reconstruction using Mg/Ca microanalysis of planktonic foraminifera *Globigerinoides ruber*, *Globigerinoides sacculifer*, and *Pulleniatina obliquiloculata*. *Paleoceanography*, *24*(3). https://doi.org/10.1029/2008pa001664

Saenger, C. P., & Evans, M. N. (2019). Calibration and validation of environmental controls on planktic foraminifera Mg/Ca using global core-top data. *Paleoceanography and Paleoclimatology*, *34*(8), 1249–1270. https://doi.org/10.1029/2018pa003507

Schiebel, R. (2002). Planktic foraminiferal sedimentation and the marine calcite budget. *Global Biogeochemical Cycles*, *16*(4), 3–1. https://doi.org/10.1029/2001gb001459

Schiebel, R., & Hemleben, C. (2017). *Planktic foraminifers in the modern ocean* (pp. 1–358). Springer.

Schiebel, R., Zeltner, A., Treppke, U. F., Waniek, J. J., Bollmann, J., Rixen, T., & Hemleben, C. (2004). Distribution of diatoms, coccolithophores and planktic foraminifers along a trophic gradient during SW monsoon in the Arabian Sea. *Marine Micropaleontology*, *51*(3–4), 345–371. https://doi.org/10.1016/j.marmicro.2004.02.001

Segev, E., & Erez, J. (2006). Effect of Mg/Ca ratio in seawater on shell composition in shallow benthic foraminifera. *Geochemistry, Geophysics, Geosystems*, *7*(2), Q02P09. https://doi.org/10.1029/2005gc000969

Shaked, Y., & Genin, A. (2016). Israel national monitroing program at the Gulf of Eilat annual report. Retrieved from http://www.iui-eilat.ac.il/Research/NMPmeteodata.aspx

Sprintall, J., & Tomczak, M. (1992). Evidence of the barrier layer in the surface layer of the tropics. *Journal of Geophysical Research*, *97*(C5), 7305–7316. https://doi.org/10.1029/92jc00407

Steiner, Z., Lazar, B., Torfstein, A., & Erez, J. (2017). Testing the utility of geochemical proxies for paleoproductivity in oxic sedimentary marine settings of the Gulf of Aqaba, Red Sea. *Chemical Geology*, *473*, 40–49. https://doi.org/10.1016/j.chemgeo.2017.10.012

Subhas, A. V., Rollins, N. E., Berelson, W. M., Erez, J., Ziveri, P., Langer, G., & Adkins, J. F. (2018). The dissolution behavior of biogenic calcites in seawater and a possible role for magnesium and organic carbon. *Marine Chemistry*, *205*, 100–112. https://doi.org/10.1016/j.marchem.2018.08.001

Tierney, J. E., Malevich, S. B., Gray, W., Vetter, L., & Thirumalai, K. (2019). Bayesian calibration of the Mg/Ca paleothermometer in planktic foraminifera. *Paleoceanography and Paleoclimatology*, *34*(12), 2005–2030. https://doi.org/10.1029/2019pa003744

Torfstein, A., & Kienast, S. S. (2018). No correlation between atmospheric dust and surface ocean chlorophyll-a in the oligotrophic Gulf of Aqaba, Northern Red Sea. *Journal of Geophysical Research: Biogeosciences*, *123*(2), 391–405. https://doi.org/10.1002/2017jg004063

Torfstein, A., Kienast, S. S., Yarden, B., Rivlin, A., Isaacs, S., & Shaked, Y. (2020). Bulk and export production fluxes in the Gulf of Aqaba, Northern Red Sea. *ACS Earth and Space Chemistry*, *4*(8), 1461–1479. https://doi.org/10.1021/acsearthspacechem.0c00079

Torfstein, A., Teutsch, N., Tirosh, O., Shaked, Y., Rivlin, T., Zipori, A., et al. (2017). Chemical characterization of atmospheric dust from a weekly time series in the north Red Sea between 2006 and 2010. *Geochimica et Cosmochimica Acta*, *211*, 373–393. https://doi.org/10.1016/j.gca.2017.06.007

Wang, L. (2000). Isotopic signals in two morphotypes of *Globigerinoides ruber* (white) from the South China Sea: Implications for monsoon climate change during the last glacial cycle. *Palaeogeography, Palaeoclimatology, Palaeoecology*, *161*(3–4), 381–394. https://doi.org/10.1016/s0031-0182(00)00094-8

Wefer, G., Berger, W. H., Bijma, J., & Fischer, G. (1999). Clues to ocean history: A brief overview of proxies. *Use of Proxies in Paleoceanography*, 1–68. https://doi.org/10.1007/978-3-642-58646-0_1

Zweng, M. M., Seidov, D., Boyer, T. P., Locarnini, M., Garcia, H. E., Mishonov, A. V., et al. (2019). World ocean atlas 2018, volume 2: Salinity.